Enhanced Polarimetric Radar Signatures above the Melting Level in a Supercell Storm

MATTHEW L. LONEY*

School of Meteorology and Cooperative Institute for Mesoscale Meteorological Studies, The University of Oklahoma, and National Severe Storms Laboratory, Norman, Oklahoma

DUŠAN S. ZRNIĆ

School of Meteorology, The University of Oklahoma, and National Severe Storms Laboratory, Norman, Oklahoma

JERRY M. STRAKA

School of Meteorology and Cooperative Institute for Mesoscale Meteorological Studies, The University of Oklahoma, and Center for Analysis and Prediction of Storms, Norman, Oklahoma

ALEXANDER V. RYZHKOV

School of Meteorology and Cooperative Institute for Mesoscale Meteorological Studies, The University of Oklahoma, and National Severe Storms Laboratory, Norman, Oklahoma

(Manuscript received 2 April 2001, in final form 16 July 2002)

ABSTRACT

Compelling in situ and polarimetric radar observations from a severe Oklahoma supercell storm are presented. The in situ observations are from an aircraft that entered the storm above the main inflow region, sampling the embryo curtain, main updraft, its western fringe (very close to the center of mesocyclonic circulation), and the hail cascade region. At the same time, the Cimarron polarimetric radar observed enhanced signatures in specific differential phase K_{dp} and differential reflectivity Z_{dr} straddling the main updraft and extending several kilometers above the melting layer. The distance of the storm from the radar balances the novelty of this dataset, however, which is on the order of 100 km. The authors therefore rely heavily on the in situ data, including calculation of polarimetric variables, on comparisons with other in situ datasets, and on accepted conceptual models of hail growth in supercell storms to clarify hydrometeor processes in light of the intriguing polarimetric signatures near the updraft. The relation of enhanced K_{dp} to the main updraft, to the Z_{dr} ''column,'' and to precipitation is discussed. Strong evidence points to melting ice particles ($>$3 mm) below the aircraft height as the origin of the K_{dp} column in the region where an abundant number of small ($<$2 mm) drops are also observed. To support the notion that these drops are shed by melting and perhaps wet growth, results of calculations on aircraft data are discussed. Resolution issues are invoked, leading to possible reconciliation of radar measurements with in situ observations.

1. Introduction

In the last decade of the twentieth century, three weather surveillance polarimetric radars with the capability to obtain and display real-time data were developed in the United States. These are the Cimarron radar of the National Severe Storms Laboratory (NSLL), the Colorado State University–University of Chicago and Illinois State Water Survey (CSU-CHILL) radar operated by the Colorado State University, and the S-band Doppler dual-polarization (S-Pol) radar at the National Center for Atmospheric Research. All three operate at a 10-cm wavelength and employ alternate horizontal and vertical polarizations as suggested by Seliga and Bringi (1976) for measurement of differential reflectivity. Calculation procedure for differential propagation phase was suggested by Mueller (1984) and a processing scheme to obtain, simultaneously, specific differential phase K_{dp} and Doppler spectral moments was proposed by Sachidananda and Zrnić (1987). The addition of cross-correlation coefficient between horizontal (H) and vertical (V) returns was given by Balakrishnan and Zrnić (1990b); it has been implemented on the Cimarron radar of the NSSL (Zahrai and Zrnić 1993). Scientists at Colorado State University have

* Current affiliation: Meteorological Service of Canada, Vancouver, British Columbia, Canada.

Corresponding author address: Dr. Dušan S. Zrnić, National Severe Storms Laboratory, 1313 Halley Circle, Norman, OK 73069.
E-mail: zrnic@nssl.noaa.gov

also used the scheme (Bringi et al. 1996) and have since tested simultaneous transmission and reception of H and V returns on the CSU-CHILL radar (Doviak et al. 2000). The National Center for Atmospheric Research (NCAR) upgraded their radar (S-Pol) to measure the same parameters (Lutz et al. 1995) and have added the capability to compute cross correlation between copolar and cross-polar components of the returned signal (Zahrai and Zrnić 1993).

Because each of these radars have been operational for over five years, a large amount of polarimetric data together with aircraft and surface measurements have become available. Furthermore, these data are from vastly different locations (S-Pol has been in Colorado, Kansas, Florida, Italy, and Brazil) so that opportunities abound to investigate polarimetric signatures of various precipitating systems. Embryonic progress has also been made in development of procedures for classification of hydrometeors (Straka et al. 2000; Liu and Chandrasekar 2000). To understand polarimetric signatures, to guide development of hydrometeor classification schemes, and to verify quantitative use of polarimetric information, there is dire need for in situ information.

The dataset analyzed herein is the first simultaneous in situ and radar survey of phenomena associated with observed ''columns'' of differential reflectivity Z_{dr} and K_{dp} in a supercell storm (Hubbert et al. 1998). The measurements were made in an Oklahoma convective storm, a type that often features both warm- and cold-rain processes and production of hail. Interpretation and comparison of these data present the usual challenge posed by the vastly different sizes of the aircraft and radar sampling volumes. The large distance of this storm from the radar ($\sim$110 km) further enhances this problem. Little has been done to verify polarimetric signatures at ranges larger than about 60 km. While an unintended side benefit arises from this dataset (which has definitive bearing on the information on the utility of polarimetric variables at large range), it is recognized that the decreased resolution of the radar signatures hinders the clarity of conclusions drawn about processes on the storm scale.

In this study, we 1) attempt to contribute to verification of dual-polarization radar measurements through association with in situ hydrometeor measurements, and 2) compare and contrast the findings from this dataset with those that motivated the hypothesis made by Hubbert et al. (1998) concerning the column of K_{dp}. These authors suggest that the column was associated with drops of median size of 0.5–2 mm produced by the melting of ice particles (graupel and hail) larger than about 9 mm. [Similar signatures might be expected in regions with shedding during wet growth of hailstones $>$9 mm (Rasmussen and Heymsfield 1987b)]. As an aside, we evaluate the merits and limitations of these particular multiparameter measurements at considerable range from the radar.

In section 2, we look at the 17 May 1995 storm and its environment and examine data-related issues. The results of the analysis are presented in section 3. Section 4 focuses on interpretation of polarimetric measurements, and conclusions are in section 5.

2. Storm environment and data issues

The in situ measurement is provided by the T-28 aircraft penetrating a supercell storm that produced severe wind and hail in northeast Oklahoma on 17 May 1995. The storm formed in Kingfisher County at the intersection of the dryline and an outflow boundary at about 1930 UTC (Fig. 1). It was observed during the Measure, Interpret, and Ground-truth Hydrometeors in Thunderstorms (MIGHT) project (Detwiler et al. 1996) and the Verification of the Origins of Rotation Experiment (VORTEX; Rasmussen et al. 1994). The CAPE determined from a special 1800 UTC balloon sounding in Norman, Oklahoma, (approximately 200 km south in the inflow ahead of storm initiation) was a modest 1700 J kg^{-1} (Fig. 2). Parcel and environmental freezing temperatures were near the 600-hPa level (3.5 km AGL).

Dual-polarization radar measurements were obtained with the NSSL's Cimarron radar. For the first hour after formation, the storm, though severe, maintained multicellular structure. Thereafter, it was supercellular, propagating west-southwest to east-northeast (from 240° toward 60°; slightly right of the mean environmental wind within the cloud layer) at 21 m s^{-1} during the time of interception (near 2120 UTC). Official observations of 2.5-cm hail were reported as well as a 40 m s^{-1} wind gust. Fortuitously, the aircraft sampled both the main updraft and its western fringe. At the time of the penetration, a tornadic vortex signature (TVS; Brown et al. 1978) was detected with the NSSL's Tornado Detection Algorithm (TDA; Mitchell et al. 1998), on the Weather Surveillance Radar-1988 Doppler (WSR-88D) at Twin Lakes, Oklahoma (KTLX). A tornado warning had been issued by the National Weather Service (NWS), though no tornado was observed. The plane flew approximately 1 km south of the mesocyclone center. This is perhaps the closest the T-28 has flown to a radar-detected TVS (A. Detwiler 1999, personal communication).

Observations were obtained at heights between 4.9 and 5.2 km (near 500 hPa; about -5°C, updraft in moist adiabatic process) where wet growth and subsequent drop shedding are theorized to occur in Oklahoma storms (Heymsfield and Hjelmfelt 1984, hereinafter referred to as HH). In situ data collected by the T-28 include temperature, vertical velocity, and liquid water content (LWC), as well as hydrometeor size and concentration from the hail spectrometer, foil impactor, and Particle Measuring Systems, Inc., (PMS) two-dimensional precipitation (2D-P) probes (Johnson and Smith 1980). About 50 s into the penetration, the 2D-P probe malfunctioned when it encountered the harsh conditions in the updraft, necessitating a heavy reliance on information from the foil impactor and hail spectrometer for

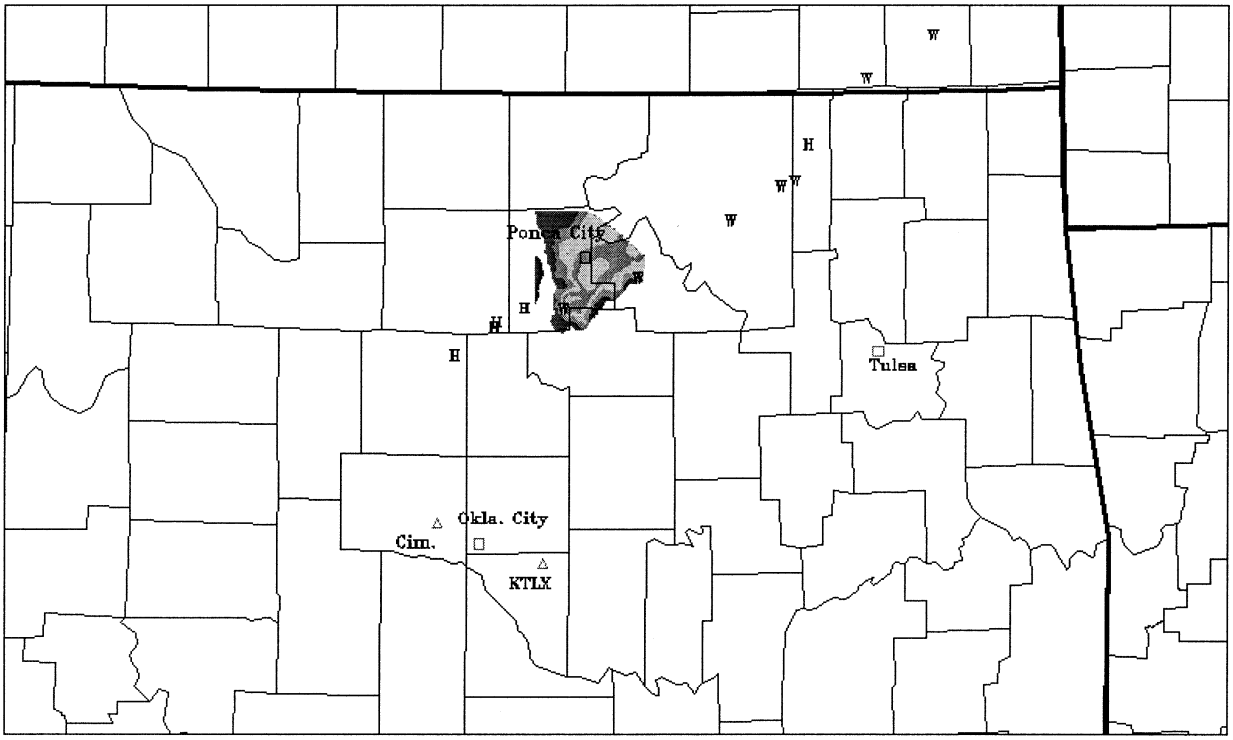

FIG. 1. Location of the 17 May 1995 storm and selected cities and radar sites. The triangle near Cim indicates the location of the Cimarron polarimetric radar, whereas the triangle near KTLX indicates the operational WSR-88D. The 2.5-km CAPPI of Z_{hh} is overlaid with hail (H) and damaging wind (W) reports. Two wind reports are partially hidden by the reflectivity contours, and two hail reports are in close proximity.

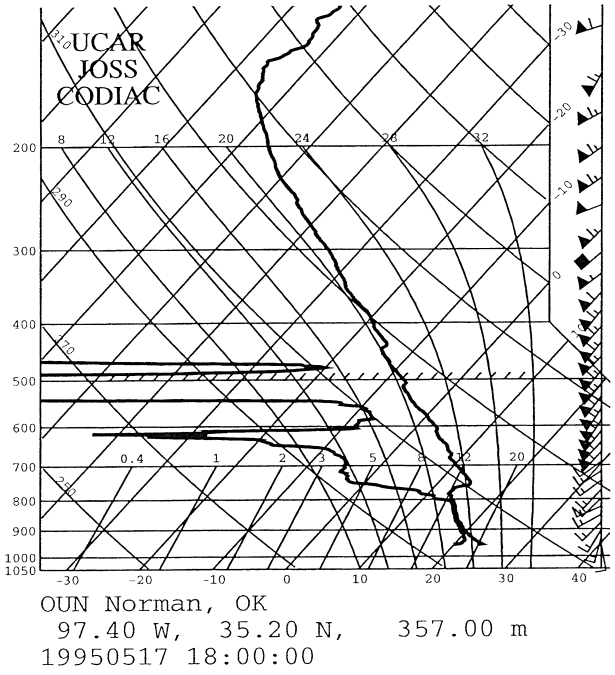

FIG. 2. Balloon sounding from Norman, OK, taken at 1800 UTC as part of VORTEX. Temperature (solid) and dewpoint temperature (dashed) are in degrees Celsius. The usual standard for wind barbs applies: flags 50, full barbs 10, and half barbs 5 kt. Freezing level corresponds to about 3.5 km AGL.

quantitative analysis thereafter (see appendix for details). Qualitative information from the 2D-P was available again approximately 40 s after the outage. The reverse-flow temperature probe provided measurement of ambient temperature.

There is inherent difficulty in associating the aircraft point measurements with the resolution volume of the radar, the two of which differ by many orders of magnitude. This is exacerbated at long ranges (~110 km) where the storm was located. The 1° beamwidth of the radar produces an effective beamwidth [which includes displacements in azimuth (Doviak and Zrnic 1993)] of 1.8–2 km. Data spacing in range was 150 m. The aircraft in this penetration flew nearly *along an azimuthal direction.* With the aircraft speed of approximately 100 m s^{-1}, it took up to 20 s to fly across each radar sample in azimuth, whereas the microphysical instruments output data every second. Thus, the worst-case scenario for data resolution comparison exists. Radar samples were taken with a 0.5° increment in elevation angle in the lowest levels up to 2.0°, and higher increments thereafter. Because the beam rises with distance under typical atmospheric conditions, the lowest height of the beam at that distance is approximately 1.6 km.

Objective analysis was performed using a modified Barnes scheme (Askelson et al. 2000). The relatively slow rate of volume scans (190 s) provided a very sparse number of truly simultaneous observations (in space and

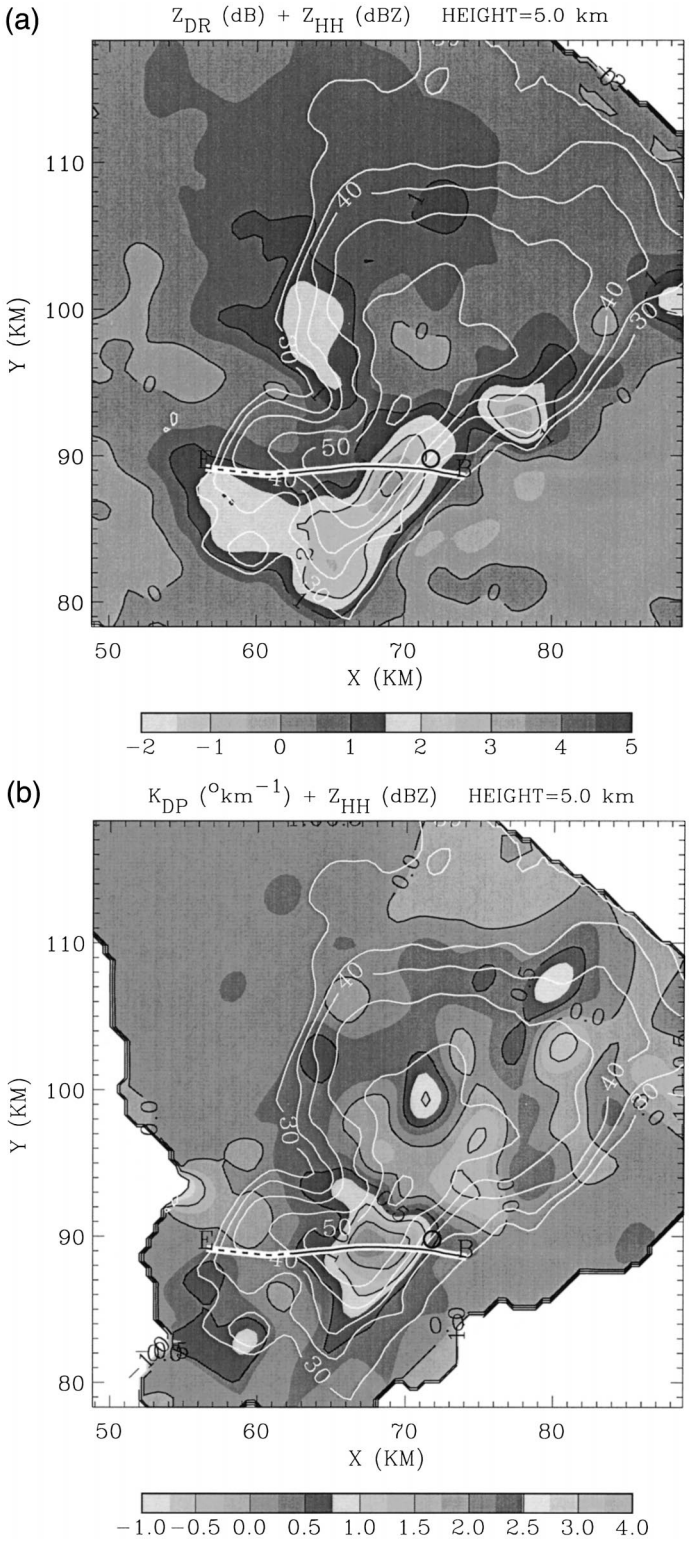

FIG. 3. (a) Contours of reflectivity factor Z_{hh} (dBZ, white curves) and differential reflectivity Z_{dr} (dB, shades given on the bar) at 5 km above ground. Data were obtained with the Cimarron radar between 2121 and 2124 UTC 17 May 1995. The aircraft track and its beginning (B, east side) and ending (E, west side) are indicated; the full line (2/3 of the track corresponding to 100 s of flight time) denotes the region from which data have been analyzed in detail. The small black circle is at the location of the mesocyclone. (b) Same as in (a) except the contours of K_{dp} (km^{-1}; indicated on the bar) are plotted.

time); hence, comparisons had to be made by assuming the fields are stationary over few minutes. Storm motion was determined and radar observations were adjusted (Gal-Chen 1982), based on the midpoint times of volume scans, to eliminate the effects of advection. The storm motion (21 m s^{-1} from 240°) was determined by the movement of the reflectivity centroid over time before and after the T-28 penetration. This was independently confirmed (within 5°) by the NSSL Storm Cell Identification and Tracking Algorithm (SCIT; Witt and Johnson 1993). Advection correction in the analysis also eliminated the apparent storm tilt that arises from nonsimultaneity of radar observations (Askelson et al. 2000). The maximum horizontal displacement due to advection at the top of the storm was ~800 m, while at the 0.5° elevation, it was ~1.9 km. The same procedure moved the aircraft track a prescribed distance based on storm motion to arrive at the optimal position for comparison of in situ measurements with the radar variables. The maximum adjustment of the track at eastern entrance of the storm was 3.5 km. At the exit of the plane from the storm, the track adjustment was ~440 m. Hence, the time axis along which in situ data are plotted is relative to the aircraft and corresponds to its flight from east to west.

3. Results of data analysis

Herein we present polarimetric radar measurements and T-28 aircraft measurements, and we introduce the hypothetical polarimetric variables that would have been measured by the aircraft based on the sampled hydrometeor distribution.

a. Cimarron polarimetric radar measurements

Reflectivity factor Z_{hh} and Z_{dr} in a constant altitude plane are depicted in Fig. 3a. The height of the CAPPI is 5.0 km AGL, approximately the height of the aircraft. Immediately evident are areas of enhanced Z_{dr} on the inflow (southern and eastern) side of the storm. Also evident to the north are the depressed values of Z_{dr} where Z_{hh} is nearly maximal, centered near $X = 71$, $Y = 97$ km. The latter is a typical signature of hail (Bringi et al. 1984; Husson and Pointin 1989; Aydin et al. 1990; Balakrishnan and Zrnić 1990a; Kennedy et al. 1995). A prominent area, in horizontal extent, of positive K_{dp} exists with values attaining 2.0° km^{-1} centered near $X = 68$, $Y = 90$ km (Fig. 3b). The aircraft entered the storm above the eastern inflow region through an area of significant Z_{hh} gradient (10 dB km^{-1}). It sampled the enhanced signature in Z_{dr} and significantly elevated values of Z_{hh} as it penetrated the southern portion of the storm. The aircraft apparently flew very close to the center of the enhanced area of K_{dp}, just ahead of the strongest reflectivity (>50 dBZ) to the west.

Vertical slices of the polarimetric variables along the aircraft track are presented in Fig. 4. These slices were constructed from the objective analysis of radar data collected on conical surfaces. Extrapolated fields below 2 km are not trustworthy because of the height of the beam at this range. Some typical signatures of a supercell are evident in Z_{hh}. To the east, above the inflow region, there is evidence of a weak-echo region (WER) at $X = 15$, $Z = 2$–4 km. Above the WER, an area of high Z_{hh} (>37 dBZ) extends eastward from the upper levels of the storm ($X = 15$, $Z = 10$ km); it represents a portion of the back-shear anvil, similar to the one in the cross section plotted by Conway and Zrnić (1993, their Fig. 17). The main precipitation shaft is evident in the interior of the storm, with high Z_{hh} extending from a height of 10 km downward to 2 km, and tilted westward with decreasing height. Depressed values of Z_{dr} are seen below the melting layer at $X = 3$–7, $Z = 3$ km. The depressed values of Z_{dr} in conjunction with high Z_{hh} (>55 dBZ in this case) denote the likely presence of hail. The aircraft enters the storm from the east ($Z = 5$ km) at a point of locally high Z_{hh}.

Each of the polarimetric variables in the slice depicts other distinct features. A prominent Z_{dr} column near $X = 13$ km protrudes approximately 2.5 km above the melting layer. Above the Z_{dr} column, an area of negative Z_{dr}, centered at $X = 10$, $Z = 9$ km, is within the 52.5-dBZ contour of Z_{hh} and just above the 55-dBZ contour. This same area is associated with a minimum in correlation coefficient ρ_{hv}, which is expected from the presence of hydrometeors in mixed phase, and possibly with irregular shapes, eccentricities and/or canting angles, signatures typical of hail (Zrnić et al. 1993). As in the CAPPI (Fig. 3b), an enhanced positive K_{dp} signature is evident in the vertical slice. The signature therefore encompasses a significant volume of the midlevel of the storm.

b. T-28 aircraft measurements and relation to radar measurements

Early in the penetration (<20 s), no liquid water was detected (Fig. 5a). This correlates well with the presence of cold air (Fig. 5b) and the measurement of strong subsidence (Fig. 6a). The value of Z_{dr} begins to increase (Fig. 6a) while K_{dp} remains near zero. Modest values of Z_{hh} between 30 and 40 dBZ occur in this interval where ρ_{hv} attains a local maximum. The concentration of small hydrometeors (for each 4.4 s of flight time, corresponding to about 440 m) increases slightly (Fig. 7a), while there are no large hydrometeors (Fig. 7b). From the preceding information (especially from the aircraft), it is expected that the small hydrometeors (Fig. 7a) in this interval are made of ice. Indeed, images from the 2D-P (not shown) confirmed the presence of small graupel with rough edges.

Cloud LWC attains a local maximum >1.5 g m^{-3} early in the flight (Fig. 5a) and is decaying in the region of moderate downdraft (~10–15 m s^{-1} between 25 and 30 s, Fig. 6a) where the temperatures rise slowly to

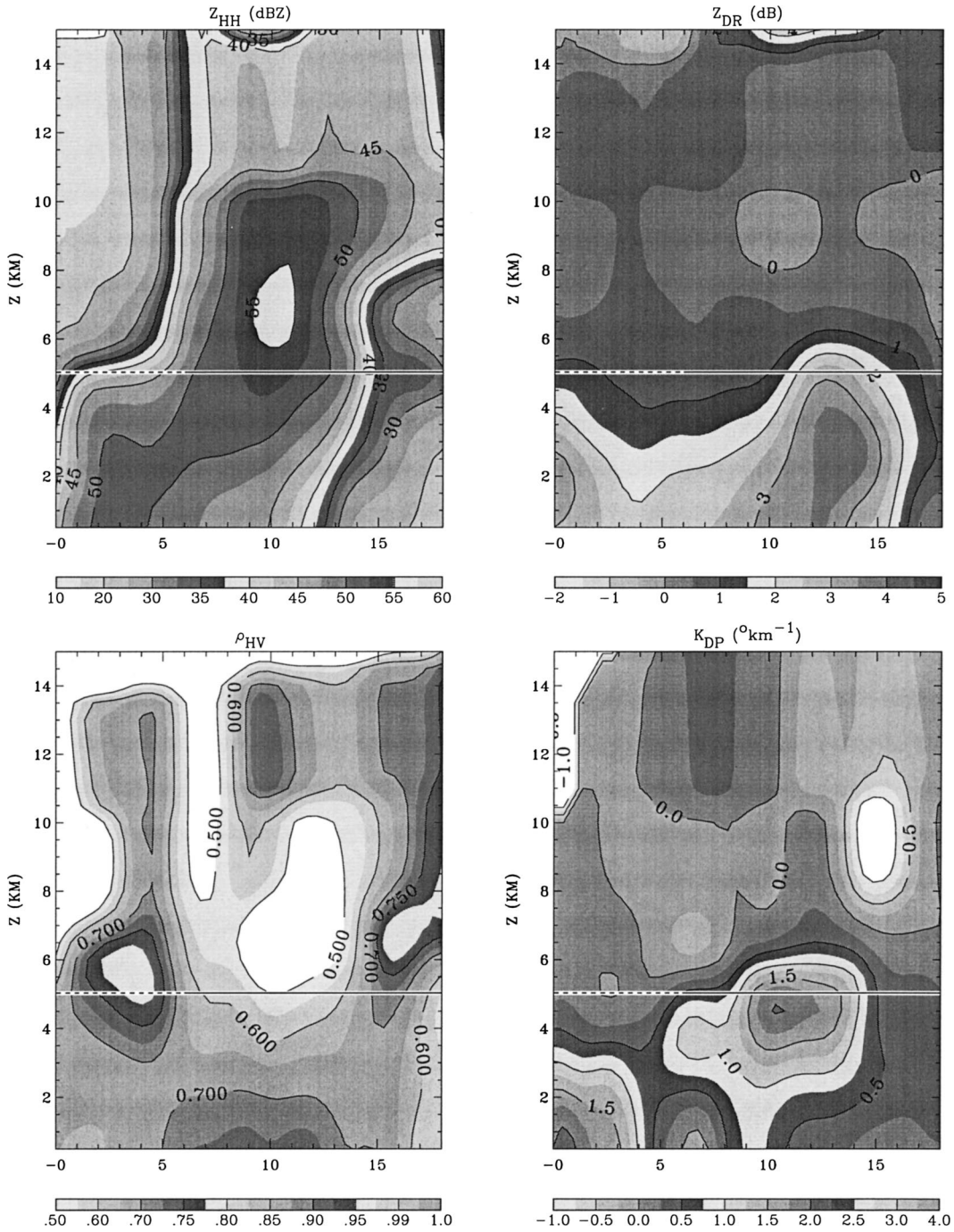

FIG. 4. Vertical cross sections of interpolated polarimetric fields. The cross sections are along the whole aircraft track and east is to the right. The aircraft track (at 5-km altitude) begins at the right; the solid line corresponds to 100 s of penetration (2/3 of total path), and that part is subsequently further scrutinized because it is centered on the enhanced Z_{dr} and K_{dp}. The horizontal dimension is compressed relative to the vertical dimension. (top left) Reflectivity Z_{hh}; (top right) differential reflectivity Z_{dr}; (bottom left) correlation coefficient ρ_{hv}; (bottom right) specific differential phase K_{dp}.

−11°C (Fig. 5b). There are few particles 1–2 mm in size (Fig. 7a) and modest concentrations of hydrometeors 5–8 mm in size (Fig. 7b). The values of Z_{hh}, Z_{dr}, and K_{dp} all exhibit significant gradients (i.e., increasing, Fig. 6), while ρ_{hv} decreases after attaining a local maximum. Small hydrometeors 1–2 mm in size decreased in concentration from 80 to 60 m^{-3} and, according to the 2D-P, had both spherical shapes (drops or frozen drops) and rough edges (small graupel). Hydrometeors 2–5 mm in size were in small concentration and were

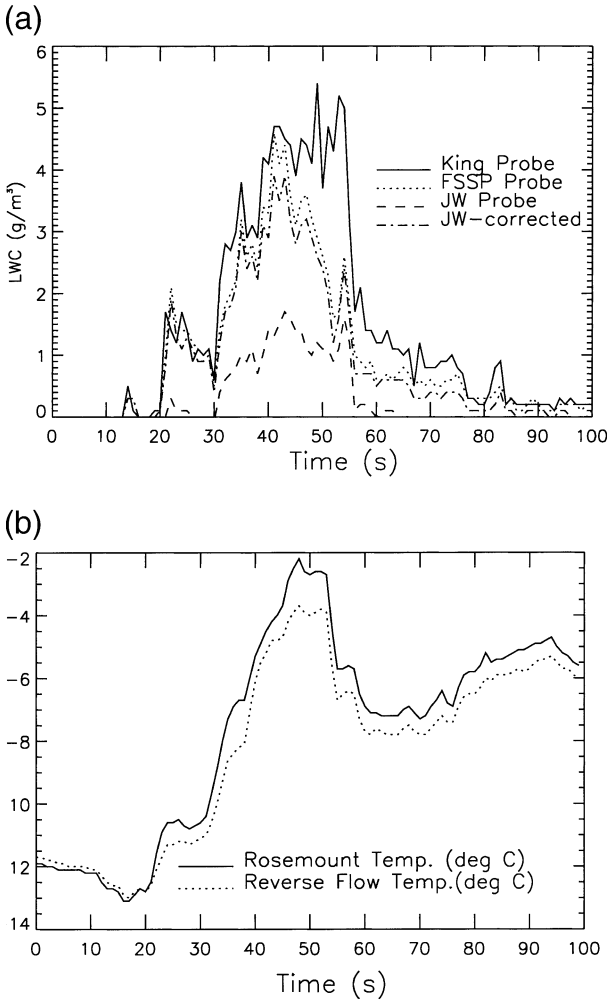

FIG. 5. (a) Liquid water content measured by probes on the aircraft along the first 2/3 of aircraft track (100 s of penetration). The path corresponding to these data is plotted with a solid line in Figs. 3 and 4 and the flight was from east to west. (b) Temperature measured by two probes aboard the aircraft.

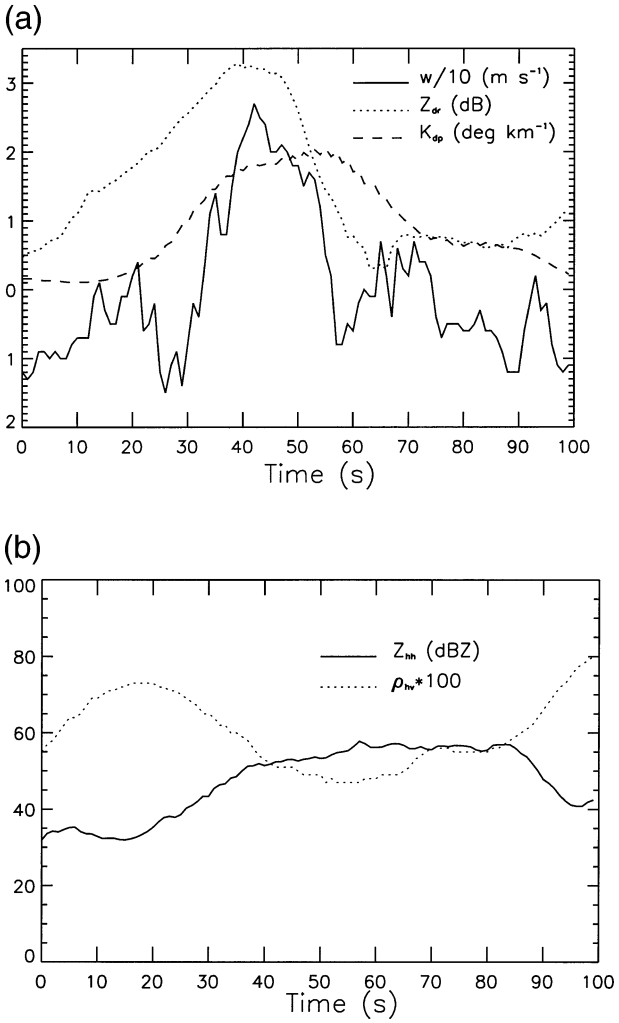

FIG. 6. (a) Updraft velocity along the first 2/3 of aircraft path (first 100 s) measured in situ and differential reflectivity and specific differential phase measured by the radar. (b) Reflectivity factor and correlation coefficient measured by the radar along the aircraft path.

mainly graupel. Larger ones (5–8 mm), with concentrations $\sim 8\ \mathrm{m}^{-3}$, were graupel and small hail.

Approximately 30 s into the penetration, the aircraft enters the main updraft of the supercell. At this time, vertical motion, LWC, and temperature all increase markedly (Figs. 5 and 6a). On the right (eastern) flank of the updraft as the aircraft flies west (30–40 s), updraft speeds are 20 m s^{-1} or less, LWC is near 3 g m^{-3}, and temperatures rise to at least -8°C (instrument lag time causes underestimation). Modest concentrations of smaller hydrometeors (5 mm or less) share space with some large (up to 8 mm) hydrometeors (Fig. 7). Larger particles (>3 mm) had imprints on the foil suggestive of graupel and small hail with both hard and slushy undefined outlines. A few of the impacts had defined edges with raised perimeters, suggestive of drops. The 2D-P images showed that the smaller hydrometeors (<3 mm) were likely drops. The value of Z_{hh} attains 50 dBZ, Z_{dr} is at its absolute maximum of 3.3 dB, and K_{dp} rises sharply to nearly 2.0° km^{-1}. The presence of a myriad of hydrometeor sizes, types, and phases found on the foil during this interval is in accord with the measured ρ_{hv}, which decreases toward its lowest value of the penetration (Fig. 6b). Note that ρ_{hv} is biased low because of quantization effect in the radar circuits for automatic gain control.

Updraft speeds (Fig. 6a) attain their maximum (>20 m s^{-1}) 39–47 s into the flight, as do temperatures (-2° to -4°C, Fig. 5), and LWC (4 g m^{-3}). There are no significant concentrations of precipitating hydrometeors of any size (save for a few 1–2 mm, Fig. 7). Both Z_{hh} and K_{dp} show continued slight increases, while Z_{dr} plateaus near 3 dB, and ρ_{hv} continues a slow decrease. On the left flank of the updraft (48–60 s), toward the interior of the storm, updraft speeds (Fig. 6a) decline again below 20 m s^{-1}, falling off abruptly between 57 and 60

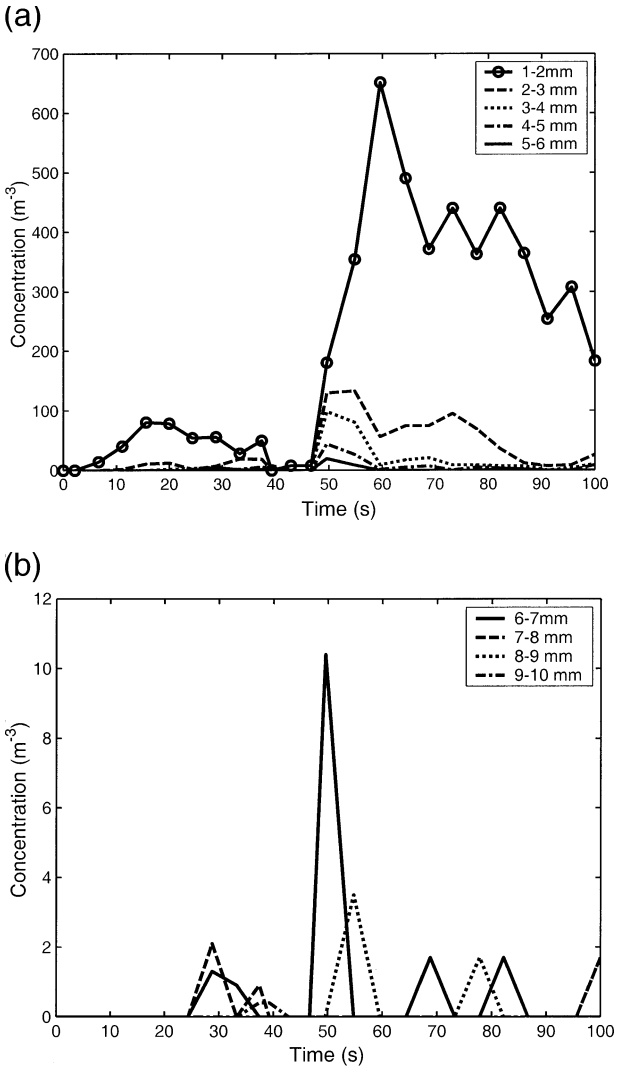

FIG. 7. Time series of concentrations (number per cubic meter) of all particles in specified size intervals along the first 2/3 of the penetration path. The data are combined from the foil impactor and hail spectrometer. (a) Size intervals are between 1 and 5 mm as indicated. (b) Size intervals are larger than 5 mm as indicated.

s. Temperatures (Fig. 5) also decrease, but not as quickly as the increase on the right flank, approaching the updraft while LWC decreases sharply from 5 to 2 g m^{-3}. An impressive jump in the concentration of detected hydrometeors occurs (Fig. 7). Especially intriguing is the first detection of particles 8 mm or larger and the abrupt rise in 1–2-mm-sized particles from 10 to >600 m^{-3}. The foil imprints from the largest of these hydrometeors have irregular shapes indicative of hail.

The T-28 enters the interior of the storm and main precipitation shaft between 60 and 90 s. At least one updraft–downdraft couplet can be seen (Fig. 6a), though downdraft values dominate overall. Temperatures (Fig. 5) begin to fluctuate slightly about −6°C while values of LWC remain below 1 g m^{-3}. Polarimetric data support hail presence; Z_{hh} (Figs. 3a and 4) maintains values >55 dBZ, while a sudden drop occurs in Z_{dr} to <1 dB followed by a rise to 1 dB. A sudden decrease also occurs in K_{dp} (Figs. 3b and 4) from 2° to <1° km^{-1}, while ρ_{hv} (Figs. 3c and 4) values remain relatively low. Hydrometeors (Fig. 7) intercepted by the aircraft include relatively high concentrations of particles 1–3 mm in diameter and modest concentrations of large hydrometeors, punctuated by 2.0-cm (73 s) and 1.2-cm (78 s) hail impacts on the foil. The 2D-P was unavailable because of its failure near the main updraft.

Beyond 100 s to the end of the penetration there was a gradual decrease of small hydrometeors (1–2 mm) and there were no hydrometeors larger than 7 mm. We next outline a shedding algorithm used to test if this process could have been ongoing near the updraft.

c. Possible role of shedding

For treatments of shedding theory, including laboratory studies and possible role in development of precipitation, the reader is referred to Carras and Macklin (1973), Rasmussen et al. (1984), Lesins and List (1986), Rasmussen and Heymsfield (1987a,b), Miller et al. (1988, 1990), and Johnson and Rasmussen (1992).

For calculations of shedding from an ice particle, we assume the existence of one source and three sinks of water mass before excess water is free to shed. Accretion of cloud water is the water mass source. The three sinks that remove water mass are 1) the Schumann–Ludlam limit (Young 1993), 2) water assumed to fill the porous lattice of the ice particle of an assumed density, and 3) accumulation of water on the surface of the hailstone in the form of a torus before shedding occurs. Model calculations and observations (HH) suggest that the lower limit of an ice particle size suitable for shedding in natural conditions (due to turbulence, hailstone tumbling, or collisional shedding) may be on the order of 5 mm.

Remaining excess water mass was converted into a number concentration of 1.5-mm-diameter drops. The updraft environment, with its high temperatures (−4°C) and LWC, would have been an excellent source of shed drops from most sizes of ice particles that might be found in or adjacent to it. Computed values at both edges of the updraft were 200–300 (m^{-3}) over 4.4-s intervals for individual hailstones. There was no appreciable difference for the considered sizes of 5, 12, and 25 mm (Loney 1999). Clearly the increase in small hydrometeor sizes (1–2 mm at time ≥ 50 s; Fig. 7a) could have been produced by shedding.

d. Polarimetric variables calculated from observed hydrometeors

It is clear that the distance of the storm from Cimarron demands further scrutiny of the behavior of polarimetric variables near the updraft of the supercell. For example,

the radar apparently fails to resolve the lack of hydrometeors (Fig. 7) in the interval between 39 and 47 s (a width of approximately 800 m), where Z_{hh} values exceed 50 dBZ (Figs. 3a and 4). Sample averaging and smoothing by the objective analysis scheme is likely to blame for these inconsistencies. The radar resolution volume, at a range of 110 km, incorporates widely spaced and diverse regions of the storm, especially important in trying to resolve areas near the updraft. Herein, attempts are made to explain these inconsistencies.

We focus on the updraft region and its periphery, because there the polarimetric signatures are strong and hydrometeor types from foil images could be better identified. In situ data are used to compute Z_{dr} and K_{dp} along the flight track. Details of how the concentrations and phases of hydrometeors were deduced are in the appendix. Images on the foil permit reasonable classification for particles in the range of 3–6 mm. Outside of this range we extrapolated to smaller and larger sizes (see the appendix). We are confident in our ability to discriminate pure rain, mixed-phase, and ice hydrometeors. However, it is not possible to directly determine the shape or orientation of these particles. Thus, for rain drops we assume the Pruppacher and Beard (1970) axis ratio

$$a/b = 1.03 - 0.062D. \quad (1)$$

For mixed-phase hydrometeors we also assume this relation. All ice hydrometeors are modeled as spherical and very wet (dielectric constant of water). By including and/or excluding different combinations of hydrometeor sizes and types, we are able to determine how these influence the computed polarimetric variables.

The fractions of hydrometeors classified as pure rain are plotted in Fig. 8a from aircraft entry until 100 s into the penetration. Recall (from the appendix) that visual classification was possible from the foil data at sizes larger than 3 mm. The first three categories are merged into one (1–4 mm) as the fractions are the same because of extrapolation. Note that there are no drops larger than 5 mm. Figure 8b depicts the fraction of the sum, rain plus mixed-phase hydrometeors, hereinafter called augmented rain. As stated in section 3b, upon approaching the east side of the updraft (35–40 s), most hydrometeors were found to be composed of liquid, whereas at the exit (west side, 50–60 s) mixed-phase particles were dominant. Extrapolation to larger sizes can be recognized by the similarity of fractions between the 4–5- and 5–6-mm category. Shortly, it will be argued that this extrapolation up one size is inconsequential for the main conclusions of this exercise.

Fractions of pure rain and mixed-phase hydrometeors are pertinent for computations of K_{dp}, whereas these two types, and ice, influence Z_{dr}.

Here Z_{dr} was obtained from the reflectivity factors at horizontal and vertical polarizations Z_h and Z_v. In our model Z_h was obtained as

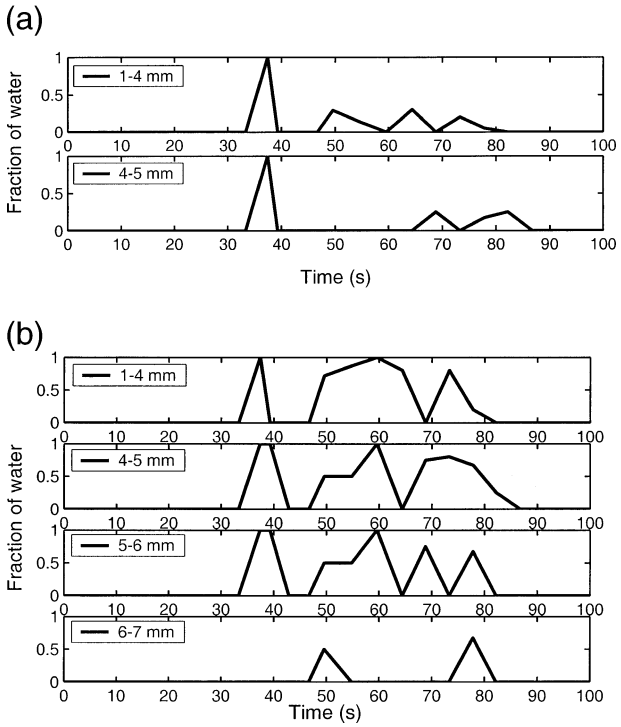

FIG. 8. Fraction of (a) raindrops in two size intervals (no rain was observed at sizes larger than 5 mm) along the first 2/3 of the flight path; and (b) fraction of the number of drops and oblate mixed-phase hydrometeors along the flight path.

$$Z_h = Z_{hw} + Z_i, \quad (2)$$

where Z_{hw} (water) was computed assuming oblate spheroidal particles and their usual backscattering cross sections (Doviak and Zrnic 1993; Stapor and Prat 1984). The fractions of hydrometeors (in various categories) contributing to Z_{hw} are in Fig. 8b. The remaining number of hydrometeors was used to compute Z_i.

A significant number of particles on the edge of the updraft and in the interior of the storm (especially with $D > 4$ mm) were noted from the foil and the 2D-P to have axis ratios $a/b \geq 1$, indicative of ice particles. If these particles were dry, their contribution to either K_{dp} or Z_{dr} would be insignificant. If they were wet and vertically oriented (an unlikely possibility), a reduction in Z_{dr} would occur (and in a direction favorable to our interpretation of data, that is, reduced Z_{dr} on the west side of the updraft). To simplify the analysis we have assumed that all such particles (detected as ice) are wet and spherical.

The value of K_{dp} was calculated from the standard formula relating forward scattering coefficients and concentrations [Doviak and Zrnic 1993, their Eq. (8.30)]. Scattering coefficients for oblate spheroids were adopted for rain as well as for mixed-phase hydrometeors.

Results of our computations coupled with the underlying assumptions allow us to infer what a polarimetric radar might see in similar situations. Qualitative com-

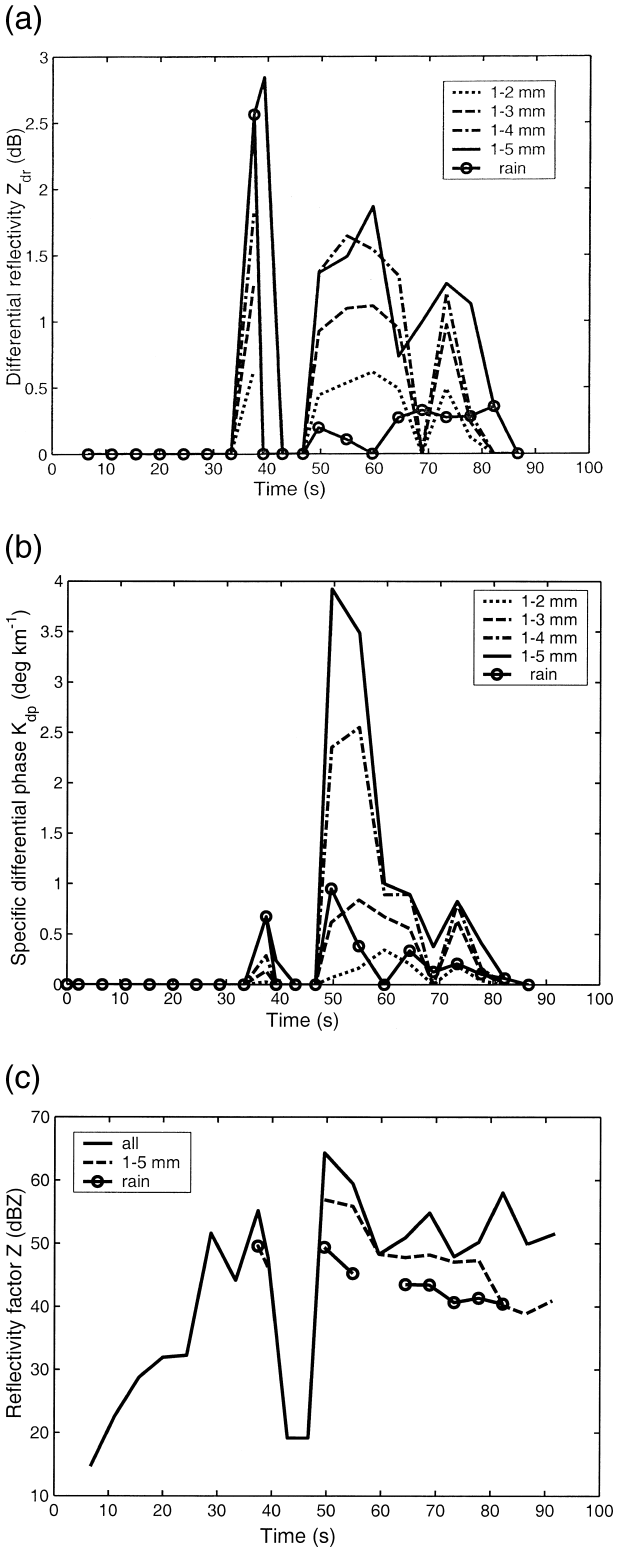

FIG. 9. (a) Time series of the computed Z_{dr} from particle concentrations along the aircraft path (first 100 s or 2/3 of the path). The rain curve contains only drops up to 5 mm, the other hydrometeors in the same category are modeled as spheres. The other curves are for augmented rain and size intervals as indicated. The ice in these size intervals is modeled as spherical and wet. (b) Time series of the computed K_{dp} under the same conditions as in (a). (c) Computed Z_{hh} for rain and augmented rain (1–5-mm size) as in (a) and for all hydrometeors in all size intervals.

parisons with our own distant observations support some of the conclusions herein. Calculated values of the polarimetric variables from the aircraft data are presented in Fig. 9.

The computed Z_{dr} (Fig. 9a) is plotted for the following two situations: 1) the rain case, whereby drops are modeled as oblate spheroids and both mixed-phase and ice particles are modeled as wet spheres, and 2) the augmented rain, where drops and mixed-phase hydrometeors are modeled as identical oblate spheroids, and ice particles are spherical.

In the rain case plot, only oblate drops up to 5 mm in size are included and mixed-phase and ice hydrometeors (also up to 5 mm in size) are lumped into water spheres. Inclusion of all hydrometeors (i.e., larger than 5 mm) caused less than 10% variation in the curve for 1–5 mm and is therefore not shown (the Z_{dr} peak reaches 3.1 dB).

The rest of the curves (Fig. 9a) represent the effects of augmented rain. For example, the dotted curve contains contributions from drops and mixed-phase hydrometeors (both oblates) and ice spheres in the size interval 1–2 mm; the dash–dot curve is contribution by all three from the size interval 1–3 mm, and so on. The point (1–5 mm) at 40 s was obtained exclusively from hail spectrometer data. The instrument registered data in categories 4–5 and 5–6 mm and there were no foil images. Since all foil images at 37 s were drops (largest sized 4–5 mm), we deduce that at 40 s the spectrometer likely detected mixed-phase hydrometeors (Fig. 10). If a spherical shape is assigned to these, the computed Z_{dr} at 40 s becomes 0, and the value at 37 s is not affected and becomes a new peak.

Obviously the distribution of sizes at the east and west sides of the updraft produces the differences in computed polarimetric variables. The relative numbers of large hydrometeors (>4 mm) primarily influence the differential reflectivity. At both 37 and 40 s the relative number of >4-mm particles is larger than at 50 or 54 s (Fig. 10) and that places the absolute maximum of Z_{dr} on the eastern flank of the updraft. The relative number of particles >4 mm is smaller at 50 and 54 s but the absolute number of particles in the range of 2–4 mm is quite large, giving the peak in K_{dp}.

4. Discussion

Analysis of the in situ data clearly indicates that hydrometeors along the flight path would likely produce peaks of Z_{dr} and K_{dp} at two disjoint locations, the right (east) and left (west) flanks of the updraft if sufficient resolution were available. Furthermore, the distribution

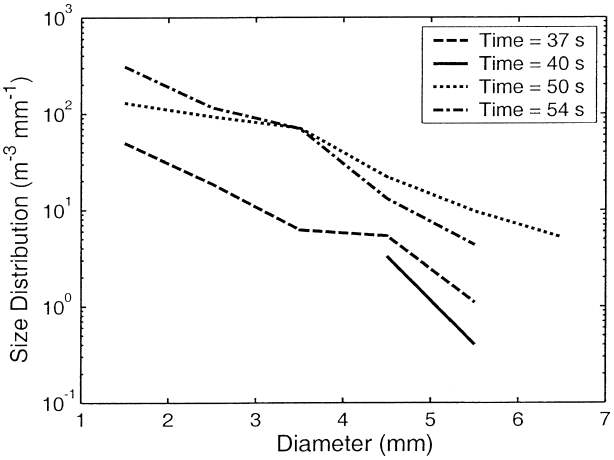

FIG. 10. Size distribution of hydrometeors at the indicated times of flight.

(Fig. 10) and type of hydrometeors encountered along the aircraft track differ significantly so that inferred polarimetric signatures would also differ. To put these findings in perspective, we begin by discussing the peaks of Z_{dr} and K_{dp} implied by computations from in situ data, followed by deliberations about signatures of Z_{dr} and K_{dp} above the freezing level. We then address implications of our in situ measurements on interpretation of polarimetric variables.

a. Peaks of calculated polarimetric variables

We focus now on the two peaks of calculated polarimetric variables on either side of the main updraft. The one on the eastern (right) flank is primarily from rain and possibly some mixed-phase particles and the second one is mostly due to mixed-phase-oriented hydrometeors. Maximums of measured Z_{dr} have been found on the eastern flanks of updrafts but have not been fully explained or confirmed by independent observations. Note that the spatial extent of the peak (augmented rain sizes 1–5 mm) exceeds 500 m, about one-fourth of the size of the radar resolution volume. It could be that the primary contribution of the measured Z_{dr} (Fig. 6a) is from these and similar hydrometeors (drops and/or drops with ice cores). Smoothing by the resolution volume would merge the second peak (if there were one) to depict a curve similar to the one in Fig. 6a.

The second peak of computed Z_{dr} (about 2 dB at 55 s in Fig. 9a) is clearly due to mixed-phase, wet hydrometeors. Our confidence that these represent the actual hydrometeors in the cloud is lower than for the case of the drops (see appendix). The computed values increase with size until the inclusion of 5-mm diameters, where they peak. For further interpretation we turn to the computed K_{dp} (Fig. 9b).

Again two peaks straddle the updraft, but this time the peak on the left (west) flank is much larger. Clearly mixed-phase oblates in the size range of 3–5 mm contribute the larger share to the peak, as the rain contribution is significantly smaller. But we also have less confidence in our ability to discern images corresponding to the mixed-phase hydrometeors. Nonetheless, it is evident that the peak due to rain on the west flank is larger than the one on the east and that addition of wet oblate spheroids would further increase it.

The radar resolves one peak in K_{dp} of 2° km^{-1} at about the right location and behind the peak in Z_{dr} (Fig. 6a). If this peak is primarily caused by hydrometeors similar to the in situ ones we submit that the dominant contributors would be oblates in the size range of 3–5 mm. In addition to beam smoothing, range averaging also reduces K_{dp}; hence, the combined effect for these data would be to diminish the values.

Computed Z_{hh} (Fig. 9c) exhibits a maximum at the same time as K_{dp} but it is due primarily to scatterers larger than 5 mm. The Z_{hh} from augmented rain (hydrometeors up to 5 mm in size) is, on the average, 5 dB lower. On the eastern flank of the updraft another peak appears. To compute reflectivity at times $<$30 s we used the refractive index of dry ice because the observations indicate that this was the phase of water. The reflectivity is consistent with the radar-observed values (Fig. 6b). Smoothing by the beam and/or contributions from other scatterers within the beam, leave no hints of the reflectivity void region. Except for the clue that hail might be present beyond 50 s, the profile of Z_{hh} gives no other indication about the hydrometeors from which it was computed.

b. Enhanced Z_{dr} above freezing level

Columns of Z_{dr} are frequently observed [see Wakimoto and Bringi (1988) for one of the first well-documented cases]. Under conditions of weak environmental shear, a thunderstorm updraft lifts moist air to the onset of condensation. Drops form (though how the large drops are formed is not well established if at all) and are lifted above the freezing level wherein they briefly exhibit positive Z_{dr}. Many previous in situ studies, including observations in multicellular and supercellular convection (Bringi et al. 1991, 1995, 1996; Brandes et al. 1995; Ramachandran et al. 1996), have supported the observation that Z_{dr} columns, usually coinciding with low Z_{hh}, are collocated, or slightly offset, with updrafts.

At the leading edges of storms we routinely observe high values of Z_{dr}. This and existence of low-precipitation storms has prompted Straka et al. (2000) to propose a separate class of rain in their hydrometeor classification scheme, the large drop rain. The observed drops of low concentration but relative deficit of small sizes, on the right flank of the updraft, corresponds to that class.

c. Enhanced K_{dp} above the freezing level

Enhanced K_{dp} above the freezing level has been observed (Hubbert et al. 1998; Zrnic and Ryzhkov 1999, their Fig. 9) and rightfully related to different causes. Ryzhkov et al. (1998, their Fig. 4) noted a deep region of enhanced values (0.3°–0.5° km^{-1}) above a high-reflectivity core, and attribute it to horizontally oriented crystals. The first comprehensive analysis of a K_{dp} column in a hailstorm was provided by Hubbert et al. (1998).

A spatial representation of the enhanced K_{dp} (Fig. 6a) in relation to the Z_{dr} column (time 30–70 s), shows the peak values of enhanced K_{dp} to be west of those of the Z_{dr} column. However, there is considerable overlap in these features. Temperatures, approximately $-4°$ to $-7°$C (Fig. 5b), and the close proximity to the updraft (measured by the T-28) suggest hydrometeors are very likely drops or wet hailstones. Furthermore, both features are offset from the reflectivity centroid, which coincides with the minimum in ρ_{hv} (Fig. 6b). The K_{dp} values peak on the western fringe of the updraft. Therefore, we have agreement with Hubbert et al. (1998, their Fig. 6) as to the placement of this enhanced K_{dp} in relation to the updraft. Specifically, it lies within the 50-dB*Z* contour (Fig. 4), but east of the Z_{hh} maximum in the reflectivity gradient region. It encompasses the interface between the main hailshaft and the fringe of the updraft and is offset west of the Z_{dr} column. However, the column in the Colorado storm protruded 1.5 km above the melting layer, whereas the ''bull's-eye'' in Fig. 4 protrudes at least 2.5 km above the melting level (the effect of beam smoothing has been accounted for).

A more columnar appearance of the K_{dp} field is evident in cross sections to the north and south of Fig. 4. Some of the details in structure are strikingly similar (Fig. 6d of Hubbert et al. 1998), although the Colorado storm was more than 2 times as close to the radar (about 35 km). As in the cited reference, the lowest ρ_{hv} is where the two features overlap and in the highest reflectivity (Fig. 6b); it suggests mixed hydrometeors or partially frozen particles (Hubbert et al. 1998; Straka et al. 2000). Furthermore, it was a persistent feature of the supercell. For approximately 30 min prior to the T-28 penetrations, but after the storm had become supercellular, consecutive volume scans showed a Z_{dr} column and enhanced K_{dp} at midlevels of the storm. The Z_{dr} column was always on the inflow side of the storm and slightly displaced from the K_{dp} feature.

d. Implications of the measurement resolution

The in situ measurements have direct bearing on interpretation of polarimetric data. The few-hundred-meters resolution along the flight path indicates that at least a similar spatial resolution of radar measurement is needed to measure the variety of type and sizes, especially near an updraft or melting level. Although the strength and size of the Oklahoma storm produce remarkable polarimetric signatures at a range >100 km, these literally tell half of the story. Namely, there is association of a well-defined Z_{dr} column protruding 2.5 km above the freezing level with the WER and main updraft. The maximum in K_{dp} is offset west from the one in Z_{dr}, otherwise the regions of enhancement overlap. However, there is no hint that two entirely different hydrometeor populations, separated by an updraft, could have produced these peaks. Without a priori knowledge about the bulk distribution of hydrometeors within the resolution volume, a self-consistency of polarimetric variables can not be established.

Limitations of polarimetric data at this range include a bias toward higher values of Z_{hh} on the edges of the storm (within ~2 km, width, of a sample in azimuth). In addition, the Z_{hh} gradient is significantly smoothed because of sample averaging and the interpolation scheme of the objective analysis. There might also be biases in K_{dp} due to nonuniform beam filling along propagation paths (Ryzhkov and Zrnic 1998). Nonetheless, polarimetric measurements did a satisfactory job of capturing the overall features.

To resolve significant bulk hydrometeor properties in supercell storms, sampling sizes of a few hundred meters are needed. That can be achieved at close range (~30 km) with a 1° beamwidth. For studying smaller storms even finer resolution is desirable. Such high resolution might not be economical for operational use. Nonetheless, we believe that signatures with degraded resolution might be extremely valuable. One can capitalize on the combined knowledge of storm structure and microphysics to infer the subresolution volume processes and their location. This is analogous to the relation between a tornadic vortex signature and the mesocyclone. Algorithms exist to detect mesocyclones and TVSs, but small tornadoes at distant ranges cannot be resolved. At over 100-km range, mesocylones are detectable in the storm midlevels and scientists are searching for clues to tell if a tornado or damaging winds are likely to occur.

5. Conclusions

Simultaneous measurements by an instrumented aircraft and a polarimetric radar were made through a high-reflectivity region in a supercell storm. The region contained a column of differential reflectivity and a column of specific differential phase. At the onset of this study, we aimed to describe the first simultaneous in situ and radar observations of an enhanced K_{dp} region above freezing level in a supercell storm. Upon further investigation, it became apparent that a blank point-by-point comparison of polarimetric radar data with in situ measurements conceals more than it reveals about the relation between the two. The size of the radar resolution volume was such that it encompassed regions with sig-

nificantly different hydrometeors. Hence, we computed Z_{hh} Z_{dr}, and K_{dp} from the in situ observations and drew the following inferences:

- A radar with a resolution of about 400 m would have observed two distinct regions of enhanced Z_{dr} and K_{dp}. One occurs on the eastern flank of the updraft where Z_{dr} has a primary peak and K_{dp} has a secondary peak, and one occurs on the western flank where the roles are reversed.
- The eastern flank contains fewer hydrometeors and there is a relative deficit of small particles (1–3 mm) in comparison with the hydrometeor-abundant western flank. Consequently, computed Z_{dr} peaks on the eastern flank and is due primarily to the larger sizes (3–5 mm).
- The western flank exhibits a peak in K_{dp}, primarily due to >2-mm sizes.
- Although the >2-mm watery particles are main contributors to the computed K_{dp} peak, the concentration of smaller sizes (1–2 mm) is at least 2 times as large as the concentration of the remaining larger sizes.

A large increase of 1–2-mm impacts on the foil coincident with hailstones >5 mm suggests a region of shedding hailstones at the western fringe of the main updraft in the 17 May 1995 storm. Microphysical calculations indicate that the updraft core and fringes were a favorable area for shedding hailstones. Sedimentation of shed drops away from the main core of the updraft into more quiescent vertical motion is a possible explanation for the large increase of 1–2-mm particles on the updraft fringe and storm interior. The probability of freezing of these drops and dominant contributors (>2 mm) increases with distance away from the high LWC and temperatures of the updraft; this can explain the columnar appearance in the K_{dp} data.

The radar-observed structures of K_{dp} and Z_{dr} columnar fields are strikingly similar to the recently reported ones in Colorado (Hubbert et al. 1998) despite the fact that our observations were at a much larger distance. Although smoothing by the beam is notably increased, the size of the structures (both in the vertical and horizontal directions) is over 2 times as large in the Oklahoma storm so that principal features are well resolved. Nevertheless, in situ data reveal details that are masked by the averaging within the radar resolution volume; computed polarimetric variables averaged over the size of the radar resolution volume replicate the enhancement in K_{dp} and Z_{dr}.

In both the Oklahoma and Colorado storms the column in Z_{dr} is east of the one of K_{dp} and is at the leading edge of the cell. This might be a characteristic of supercell storms. At least in observation of an ordinary storm, the Z_{dr} and K_{dp} have been collocated (Zrnic et al. 2001).

The abundant number of drops in the size range of 1–2 mm, detected by the foil impactor on the western flank of the updraft, is in accord with the Hubbert et al. (1998) inference, that is, that these are shed from hailstones. Nonetheless, the interpretation of the in situ data as it relates to the polarimetric signatures adds the following nuance unaccounted for in the cited reference: the in situ measurements imply that the enhancement of K_{dp} is principally due to wet-oriented particles >2 mm in diameter. If these measurements are representative over the radar resolution volume, then the K_{dp} column is an indirect manifest of the shedding process (i.e., large number of small 1–2-mm drops) and not an effect of small drops as hypothesized by Hubbert et al. (1998). Nonetheless, it is remarkable that, without the aid of in situ measurements, these authors infer the essence and location of this important microphysical process in the Colorado storm. Our in situ measurements indicate that the overlap between the two columns could be due to poor radar resolution, otherwise there would be two enhancements of each, Z_{dr} and K_{dp}. Similar effect might be present in the Hubbert et al. (1998) data.

To resolve polarimetric signatures, comparable to in situ inferred ones, requires a sampling size smaller than about 400 m. Such fine resolution can be achieved across the beam for storms relatively close to the radar. At the moment, high-resolution K_{dp} data in range are very noisy and need smoothing for reliable interpretation. Moreover, longer dwell times and/or alternate methods to process the other polarimetric variables are required to obtain resolution compatible to the phenomena without sacrificing accuracy of estimates.

Clearly, there is yet no substitute for in situ measurements, both in resolution and specifics of information, concerning hydrometeors. These measurements also provide finely resolved details about expected behavior of polarimetric variables. We wish that the opposite were true for the fields of observed polarimetric variables (i.e., provide fine details about hydrometeors). Nonetheless, the latter do reveal regions wherein important microphysical processes occur. As shown, processes affecting scales smaller than the radar resolution volume, can produce signatures in the polarimetric variables. But interpretation of these without additional information is difficult at best, impossible at worst.

To fully capitalize on polarimetric measurements, researchers need to devise fast volume scans (<1 min) and observe with a resolution of few hundred meters. This can be achieved with conventional radar by probing small sectors. Then time-lapse fields of polarimetric variables could provide information eclipsing that available from conventional trajectory analysis. The two together might revolutionize the science of bulk microphysics and improve parameterization in numerical models.

Acknowledgments. This work evolved from an M.S. thesis by the lead author at The University of Oklahoma. We thank Andrew Detwiler, Dennis Musil, and Paul Smith from the South Dakota School of Mines and Technology for all of their help, and Mark Askelson, Paul Schlatter, and Christopher Curtis for their assistance.

Four anonymous reviewers provided helpful suggestions for the manuscript. Partial funding for this work was supported by NSF Grants ATM 9311911, 9120009, 9671318. The first author was supported by a National Aeronautics and Space Administration grant to the NSSL and the Cooperative Institute for Mesoscale Meteorological Studies.

APPENDIX

Determination of Hydrometeor Type and Number

The particle-size distribution (PSD) was obtained by combining data from the hail spectrometer and foil impactor (the 2D-P was unavailable for quantitative analysis). The foil was split into 6-in segments (4.4 s of flight time) and meticulously analyzed. The hail spectrometer data (sampled every second) was then appropriately added to this coarser temporal and spatial sampling interval (the sample volume of the hail spectrometer is about 10 times as large as that of the foil impactor). This merging of data has influence only on sizes larger than the smallest size (4 mm) available from the spectrometer.

The diameter D was determined from the foil by adding the major and minor axis of the largest particles (>4 mm) and dividing by 2, giving an average value, and then placing it in the appropriate 1-mm-wide bin with the hail spectrometer data. Note that nonspherical particles were either ice or mixed phase and for these the estimated diameter is slightly larger than the equal volume diameter. Further, the drop impact leaves a slightly larger diameter. To correct for this effect we assumed a relation proposed by Schecter and Russ (1970) and used in similar circumstances by Brandes et al. (1995):

$$0.89\, D_f = D, \tag{A1}$$

where D_f is the imprint diameter (in the foil) and D is the correct diameter. This relation is a good correction up to and including 4–5-mm categories. Nonetheless the correction had insignificant effect on the concentrations.

Sizes were sorted into 1-mm increments starting with 1 mm. We did not attempt to determine from the foil the phase of spherical hydrometeors in the lower two categories (1–2 and 2–3 mm). We refer to Knight et al. (1977), who found that the distinction between spherical particles, be they liquid, solidly frozen, or slushy, was difficult and often impossible at diameters ≤ 3 mm. However, they found that distinction between rime, including slushy rime, and solid ice or liquid particles is unambiguous, both by imprint shape and by uneven borders or molding of the grooves. For larger categories the imprints could be partitioned into those caused by drops (smooth and circularly symmetric), mixed phase (some rough spots and splatter), and ice particles (rough edges and noncircular shape).

To obtain the numbers of water drops in each category, the following procedure was adopted. The percent of drops in the 3–4-mm category determined from the foil was extrapolated directly to the 2–3- and 1–2-mm categories. This can underestimate the water part in these categories, if the liquid fraction in the 3–4-mm category is smaller than 1, because a larger proportion of smaller hydrometeors (1–3 mm) would melt in the updraft.

The hail spectrometer does not discriminate between hydrometeor type; hence, extrapolation from the foil was made to determine the proportion of rain or mixed phase in the same size category. Furthermore, there were times when the categories larger than 5 mm had only data from the spectrometer. In that case two possibilities were tested. One, the data were assumed to be spherical hail, and two, if that category was one size larger than the category available from the foil, extrapolation was used.

The contribution to the polarimetric variables by ''pure'' rain could underestimate significantly the actual contribution. This is because pure rain excludes mixed-phase particles. These have the refractive index of water and are likely oriented. For that reason, computations were done whereby the total number of water drops included the mixed phase as well, the so-called augmented rain. The same type of extrapolation of mixed-phase particles as for pure drops was made to smaller and larger categories, with one exception at one point in time. We have assigned the rain fraction from the foil (37-s data) to the mixed-phase fraction of spectrometer data at 39 s. At 37 s, all 3–4- and 4–5-mm foil impacts were from pure rain. As there was no foil data at 39 s whatsoever we assigned the rain fractions to the mixed-phase fractions in the same category. This was at the entrance to the updraft and conforms to recent measurements with a disdrometer in Oklahoma (Schuur et al. 2001, their Fig. 15) indicating that a significant number of hydrometeors even larger than 6 mm look like rain.

In all computations within the updraft, the ice hydrometeors were assumed to be wet and spherical. This has no effect on the deduced $K_{\rm dp}$ but tends to suppress the $Z_{\rm dr}$ values.

To give the reader a qualitative sense for the accuracy of our procedure, we rank in order of decreased confidence the various parameters we deduced about the hydrometeors. The total number of hydrometeors ranks first; it amounts to counting and is better than the tally in the 2000 Florida presidential election. The number by size category is second, with an error of about 10%. Determination of phase ranks third. We expect that the number of pure drops is smaller than the actual number of hydrometeors the radar would sense as drops. That is because many drops with ice cores are classified as mixed phase. Hence, on the whole, the computed polarimetric signatures would have a deficit. Similarly a barely wet hydrometeor would appear as ice and yet could be horizontally oriented and act as a drop.

REFERENCES

Askelson, M. A., J. P. Aubagnac, and J. M. Straka, 2000: An adaptation of the Barnes filter applied to the objective analysis of radar data. *Mon. Wea. Rev.,* **128,** 3050–3083.

Aydin, K., Y. Zhao, and T. A. Seliga, 1990: A differential reflectivity radar hail measurement technique: Observations during the Denver hailstorm of 13 June 1984. *J. Atmos. Oceanic Technol.,* **7,** 104–113.

Balakrishnan, N., and D. S. Zrnić, 1990a: Estimation of rain and hail rates in mixed-phase precipitation. *J. Atmos. Sci.,* **47,** 565–583.

——, and ——, 1990b: Use of polarization to characterize precipitation and discriminate large hail. *J. Atmos. Sci.,* **47,** 1525–1540.

Brandes, E. A., J. Vivekanandan, J. D. Tuttle, and C. J. Kessinger, 1995: A study of thunderstorm microphysics with multiparameter radar and aircraft observations. *Mon. Wea. Rev.,* **123,** 3129–3143.

Bringi, V. N., T. A. Seliga, and W. A. Cooper, 1984: Analysis of aircraft hydrometeor spectra and differential reflectivity (Z_{dr}) radar measurements during the Cooperative Convective Precipitation Experiment. *Radio Sci.,* **19,** 157–167.

——, D. A. Burrows, and S. M. Menon, 1991: Multiparameter radar and aircraft study of raindrop spectral evolution in warm-based clouds. *J. Appl. Meteor.,* **30,** 853–880.

——, K. Knupp, and L. Liu, 1995: Microphysical and kinematic study of early-to-mature cloud transition using multiparameter radar, dual-Doppler synthesis and aircraft penetrations. Preprints, *Conf. on Cloud Physics*, Dallas, TX, Amer. Meteor. Soc., 267–271.

——, L. Liu, P. C. Kennedy, V. Chandrasekar, and S. A. Rutledge, 1996: Dual multiparameter radar observations of intense convective storms: The 24 June 1992 case study. *Meteor. Atmos. Phys.,* **59,** 3–31.

Brown, R. A., L. R. Lemon, and D. W. Burgess, 1978: Tornado detection by pulsed Doppler radar. *Mon. Wea. Rev.,* **106,** 29–38.

Carras, J. W., and W. C. Macklin, 1973: The shedding of accreted water during hailstone growth. *Quart. J. Roy. Meteor. Soc.,* **99,** 639–648.

Conway, J. W., and D. S. Zrnić, 1993: A study of embryo production and hail growth using dual-Doppler and multiparameter radars. *Mon. Wea. Rev.,* **121,** 2511–2528.

Detwiler, A. G., K. R. Hartman, and P. L. Smith, 1996: Summary of T-28 participation in VORTEX/MIGHT, 1994–1995. Rep. SDSMT/IAS/R-96/01, South Dakota School of Mines, 108 pp.

Doviak, R. J., and D. S. Zrnić , 1993: *Doppler Radar and Weather Observations.* 2d ed. Academic Press, 562 pp.

——, V. Bringi, A. Ryzhkov, A. Zahrai, and D. S. Zrnić, 2000: Considerations for polarimetric upgrades to operational WSR-88D radars. *J. Atmos. Oceanic Technol.,* **17,** 257–278.

Gal-Chen, T., 1982: Errors in fixed and moving frame of references: Applications for conventional and Doppler radar analysis. *J. Atmos. Sci.,* **39,** 2279–2300.

Heymsfield, A. J., and M. R. Hjelmfelt, 1984: Processes of hydrometeor development in Oklahoma convective clouds. *J. Atmos. Sci.,* **41,** 2811–2835.

Hubbert, J., V. N. Bringi, and L. D. Carey, 1998: CSU-CHILL polarimetric measurements from a severe hailstorm in eastern Colorado. *J. Appl. Meteor.,* **37,** 749–775.

Husson, D., and Y. Pointin, 1989: Quantitative estimation of hailfall intensity with a dual-polarization radar and a hailpad network. Preprints, *24th Conf. on Radar Meteorology,* Tallahassee, FL, Amer. Meteor. Soc., 318–321.

Johnson, D. B., and R. M. Rasmussen, 1992: Hail growth hysterisis. *J. Atmos. Sci.,* **49,** 2525–2532.

Johnson, G. N., and P. L. Smith Jr., 1980: Meteorological instrumentation system on the T-28 thunderstorm research aircraft. *Bull. Amer. Meteor. Soc.,* **61,** 972–979.

Kennedy, P. C., V. N. Bringi, S. Bolen, and S. A. Rutledge, 1995: An examination of dual polarization signatures associated with confirmed occurrences of large hail. Preprints, *27th Conf. on Radar Meteorology,* Vail, CO, Amer. Meteor. Soc., 41–43.

Knight, C. A., N. C. Knight, W. W. Grotewold, and T. W. Cannon, 1977: Interpretation of foil impactor impressions of water and ice particles. *J. Appl. Meteor.,* **16,** 997–1002.

Lesins, G. B., and R. List, 1986: Sponginess and drop shedding of gyrating hailstones in a pressure-controlled icing wind tunnel. *J. Atmos. Sci.,* **43,** 2813–2825.

Liu, H., and V. Chandrasekar, 2000: Classification of hydrometeors based on polarimetric radar measurements: Development of fuzzy logic and neuro-fuzzy systems, and in-situ verification. *J. Atmos. Oceanic Technol.,* **17,** 140–164.

Loney, M. L., 1999: In-situ and multiparameter radar observations of an isolated Oklahoma super-cell at far range. M.S. thesis, Dept. of Meteorology, University of Oklahoma, 152 pp.

Lutz, J., P. Johnson, B. Lewis, E. Loew, M. Randall, and J. VanAndel, 1995: NCAR's SPOL portable polarimetric S-band radar. Preprints, *Ninth Symp. on Meteorological Observations and Instrumentation,* Charlotte, NC, Amer. Meteor. Soc., 408–410.

Miller, L. J., J. D. Tuttle, and C. A. Knight, 1988: Airflow and hail growth in a severe northern high plains supercell. *J. Atmos. Sci.,* **45,** 736–762.

——, ——, and G. B. Foote, 1990: Precipitation production in a large Montana hailstorm: Airflow and particle growth trajectories. *J. Atmos. Sci.,* **47,** 1619–1646.

Mitchell, E. D., S. V. Vasiloff, G. J. Stumpf, A. Witt, M. D. Eilts, J. T. Johnson, and K. W. Thomas, 1998: The National Severe Storms Laboratory Tornado Detection Algorithm. *Wea. Forecasting,* **13,** 352–366.

Mueller, E. A., 1984: Calculation procedure for differential propagation phase shift. Preprints, *22d Conf. on Radar Meteorology,* Zurich, Switzerland, Amer. Meteor. Soc., 397–399.

Pruppacher, H. R., and K. V. Beard, 1970: A wind tunnel investigation of the internal circulation and shape of water drops falling at terminal velocity in air. *Quart. J. Roy. Meteor. Soc.,* **96,** 247–256.

Ramachandran, R., A. Detwiler, J. Helson Jr., and P. L. Smith, 1996: Precipitation development and electrification in Florida thunderstorm cells during Convection and Precipitation/Electrification Project. *J. Geophys. Res.,* **101** (D1), 1599–1619.

Rasmussen, E. N., J. M. Straka, R. Davies-Jones, C. A. Doswell III, F. H. Carr, M. D. Eilts, and D. R. MacGorman, 1994: Verification of the Origins of Rotation in Tornadoes Experiment: VORTEX. *Bull. Amer. Meteor. Soc.,* **75,** 995–1006.

Rasmussen, R. M., and A. J. Heymsfield, 1987a: Melting and shedding of graupel and hail. Part I: Model physics. *J. Atmos. Sci.,* **44,** 2754–2763.

——, and ——, 1987b: Melting and shedding of graupel and hail. Part III: Investigation of the role of shed drops as hail embryos in the 1 August CCOPE severe storm. *J. Atmos. Sci.,* **44,** 2783–2803.

——, V. Levizzani, and H. R. Pruppacher, 1984: A wind tunnel and theoretical study on the melting behavior of atmospheric ice particles: III. Experiment and theory for spherical ice particles of radius >500 μm. *J. Atmos. Sci.,* **41,** 381–388.

Ryzhkov, A. V., and D. S. Zrnić, 1998: Beamwidth effects on the differential phase measurements of rain. *J. Atmos. Oceanic Technol.,* **15,** 624–634.

——, ——, and B. A. Gordon, 1998: Polarimetric method for ice water content determination. *J. Appl. Meteor.,* **37,** 125–134.

Sachidananda, M., and D. S. Zrnić, 1987: Rain rate estimates from differential polarization measurements. *J. Atmos. Oceanic Technol.,* **4,** 588–598.

Schecter, T. A., and R. G. Russ, 1970: The relationship between inprint size and drop diameter for an airborne drop sampler. *J. Appl. Meteor.,* **9,** 123–126.

Schuur, T. J., A. V. Ryzhkov, D. S. Zrnić, and M. Schönhuber, 2001: Drop size distributions measured by a 2D video disdrometer:

Comparison with dual-polarization radar data. *J. Appl. Meteor.*, **40,** 1019–1034.
Seliga, T. A., and V. N. Bringi, 1976: Potential use of radar reflectivity measurements at orthogonal polarizations for measuring precipitation. *J. Appl. Meteor.*, **15,** 69–76.
Stapor, D. T., and T. Prat, 1984: A generalized analysis of dual-polarization measurements of rain. *Radio Sci.*, **19,** 90–98.
Straka, J. M., D. S. Zrnić, and A. V. Ryzhkov, 2000: Bulk hydrometeor classification and quantification using polarimetric radar data: Synthesis of relations. *J. Appl. Meteor.*, **39,** 1341–1372.
Wakimoto, R. M., and V. N. Bringi, 1988: Dual-polarization observations of microbursts associated with intense convection: The 20 July storm during the MIST Project. *Mon. Wea. Rev.*, **116,** 1521–1539.
Witt, A., and J. T. Johnson, 1993: An enhanced storm cell identification and tracking algorithm. Preprints, *26th Conf. on Radar Meteorology*, Norman, OK, Amer. Meteor. Soc., 154–156.
Young, K. C., 1993: *Microphysical Processes in Clouds.* Oxford University Press, 427 pp.
Zahrai, A., and D. S. Zrnić, 1993: The 10-cm-wavelength polarimetric radar at NOAA's National Severe Storms Laboratory. *J. Atmos. Oceanic Technol.*, **10,** 649–662.
Zrnić, D. S., and A. Ryzhkov, 1999: Polarimetry for weather surveillance radar. *Bull. Amer. Meteor. Soc.*, **80,** 389–406.
——, V. N. Bringi, N. Balakrishnan, K. Aydin, V. Chandrasekar, and J. Hubbert, 1993: Polarimetric measurements in a severe hailstorm. *Mon. Wea. Rev.*, **121,** 2223–2238.
——, A. Ryzhkov, J. Straka, Y. Liu, and J. Vivekanandan, 2001: Testing a procedure for automatic classification of hydrometeor types. *J. Atmos. Oceanic Technol.*, **18,** 892–913.